Applied Physics Letters ARTICLE scitation.org/journal/apl

Phase transition of $Bi_5Ti_3FeO_{15}$ ceramics discovered by Raman spectroscopy and *in situ* synchrotron XRD under stress field

Cite as: Appl. Phys. Lett. **117**, 022901 (2020); doi: 10.1063/5.0019034
Submitted: 22 June 2020 · Accepted: 29 June 2020 ·
Published Online: 13 July 2020

Mengyun Bian (卞梦云),[1] Yan Ye (叶艳),[1] Anyang Cui (崔安阳),[1] Kai Jiang (姜凯),[1,a)] Wei Bai (白伟),[2] Hongliang Dong (董洪亮),[3] Bin Chen (陈斌),[3] Zhigao Hu (胡志高),[1,4,5,b)] and Junhao Chu (褚君浩)[1,4,5]

AFFILIATIONS

[1]Technical Center for Multifunctional Magneto-Optical Spectroscopy (Shanghai), Engineering Research Center of Nanophotonics and Advanced Instrument (Ministry of Education), Department of Materials, School of Physics and Electronic Science, East China Normal University, Shanghai 200241, China
[2]Key Laboratory of Polar Materials and Devices (MOE), East China Normal University, Shanghai 200241, China
[3]Center for High Pressure Science and Technology Advanced Research, Shanghai 201203, China
[4]Collaborative Innovation Center of Extreme Optics, Shanxi University, Taiyuan, Shanxi 030006, China
[5]Shanghai Institute of Intelligent Electronics and Systems, Fudan University, Shanghai 200433, China

[a)]Electronic mail: kjiang@ee.ecnu.edu.cn
[b)]Author to whom correspondence should be addressed: zghu@ee.ecnu.edu.cn

ABSTRACT

$Bi_5Ti_3FeO_{15}$ (BTFO) ceramics have been widely studied as a multiferroic material with some potential applications. However, the effect of the stress field on BTFO ceramics with complex lattice structures is unknown. Here, we use pressure-dependent Raman scattering spectroscopy to study the structure/phase transition of BTFO samples. Because the phonon mode changes significantly, there could be a phase transition in the range of 4.5–14.8 GPa. In order to further prove the occurrence of phase transition, we carried out *in situ* high-pressure angular dispersion x-ray diffraction (XRD), which clearly proved the structural evolution of BTFO: orthorhombic crystal $A2_1am$ transformed into tetragonal $I4/mmm$. Note that the results from the XRD experiment are self-consistent with the data derived from Raman spectroscopy. It provides an effective method to explore the phase transition of complex oxide structures under high pressure.

In recent years, bismuth perovskite has been concerned because of high dielectric constant, low dielectric loss, good piezoelectric and pyroelectric properties, and so on.[1–3] The Aurivillius perovskite phase chemical formula is $(Bi_2O_2)^{2+}(A_{n-1}B_nO_{3n+1})^{2-}$, where B is a diamagnetic transition metal ion such as Ti^{4+} or Nb^{5+}, A is an alkali or alkaline earth cation, and n is the number of oxygen octahedra.[4] In Aurivillius perovskite, the phase transition process is different with different numbers of Bismuth perovskite layers. For $n=1$, $BaTiO_3$ undergoes the phase transition $Pm3m$ − $P4mm$ (120 °C) − $Amm2$ (5 °C) − $R3m$ (−90 °C) during the cooling process.[5] For $n=2$, Megaw *et al.*[6] and Nakashima *et al.*[7] have independently shown that the $A2_1am$ to $I4/mmm$ transition in $SrBi_2T_2O_9$ proceeds via an intermediate paraelectric $Amam$ phase. For $n=3$, the structural phase transition of $Bi_4Ti_3O_{12}$ ceramics changed from the orthorhombic phase ($B2eb$) to the tetragonal phase ($I4/mmm$).[4] For $n=4$, however, $Bi_5Ti_3FeO_{15}$ (BTFO) ceramics have been widely used in data storage, spin valves, spin electronic devices, sensors, and other potential applications.[3,4,8–10] The lattice structure of BTFO consists of three perovskite sample unit sandwich units growing along the c-axis between fluorite structure $(Bi_2O_2)^{2+}$ layers.[11,12] The $(Bi_2O_2)^{2+}$ layer is perpendicular to the quadruple axis of the oxygen octahedron. The Néel temperature of the BTFO film is 85 K.[1] In addition, the good fatigue resistance and lead-free properties of the BTFO ceramic make it a promising alternative to lead perovskite.[9,10]

However, the phase transition of BTFO ceramics is still controversial under the influence of external force fields. A lot of research studies have been conducted on the phase transition process of the BTFO structure. The previous results using birefringence indicate that the structure of BTFO ceramics can be transformed from $A2_1am$ to $I4/mmm$ after undergoing an intermediate phase.[13] The results of

powder neutron diffraction studies indicate that BTFO ceramics have changed from a ferroelectric orthorhombic space group $A2_1am$ to a tetragonal paraelectric phase space group $I4/mmm$, which do not exist without the mesophase.[14–16] The results of differential scanning calorimetry indicate the structural changes of BTFO: orthorhombic–tetragonal transformation and lattice expansion.[17,18] The phase transition of pure BTFO ceramics occurs when the temperature rises to Curie temperature up to 750 °C: the ferroelectric orthorhombic phase changes into the paraelectric tetragonal phase. Compared to the influence of temperature on the structure of BTFO, the effect from high pressure on the change in the lattice structure and the interaction between atoms is greater.[19] Nevertheless, there are few theoretical and experimental studies on structural changes of BTFO under high pressure. In order to fill this gap, the lattice dynamics and phase transitions process of BTFO ceramics were investigated by Raman scattering spectroscopy with the pressure up to 27.4 GPa in the present work. As we know, Raman scattering spectra are nondestructive and attractive probe techniques, which can provide some invaluable information on lattice vibrations and structural variations. Based on the analysis of the frequency, intensity, and full width at half maxima (FWHM), we observed the evolution process of the BTFO structure with the pressure. In order to verify the results of phase transition of BTFO ceramics in the pressure-dependent Raman spectra, the *in situ* high-pressure angle-dispersive x-ray diffraction (XRD) experiments are further presented. The variation trend of cell parameters under different pressures is well self-consistent with the frequency variation of phonon mode of Raman spectra.

BTFO ceramics were prepared by traditional solid phase sintering. The sample preparation process can be referred to the literature.[20] BTFO ceramics were crushed into powder with the typical size ranging from a few micrometers to tens of micrometers. A small amount of powder was loaded along with a few particles of ruby in a hole of 120 μm diameter drilled in a preindented 70 μm thick tungsten gasket of a Mao-Bell-type diamond-anvil cell (DAC). The pressure-transmitting medium was silicone oil. Raman scattering measurements were carried out with the pressure of 0–27.4 GPa at room temperature using a Jobin-Yvon LabRAM HR Evolution micro-Raman spectrometer.[21–23] The He–Ne laser with the wavelength of 632.8 nm is taken as the exciting source. The laser beam was focused through a 50× microscope with a working distance of 18 mm. An air-cooled charge-coupled device (CCD) was used to collect the scattered signal dispersed on 1800 grooves/mm grating in the frequency range of 5–1000 cm^{-1}. *In situ* high-pressure angle-dispersive XRD experiments with a wavelength of 0.6199 Å beam were carried out at beamline BL15U1, Shanghai Synchrotron Radiation Facility (SSRF), China. CeO_2 was used as the standard sample to perform the calibration. Then, XRD data were recorded using an imaging plate detector and transformed into one-dimensional XRD patterns using the DIOPTAS program. Fullprof with the WinPLOTR module was also used to calculate the cell parameters of BTFO.

Figures 1(a) and 1(b) show the pressure-dependent Raman scattering spectra of $Bi_5Ti_3FeO_{15}$ ceramics with the pressure range of 0–27.4 GPa at room temperature. The mapping of different intensities for Raman peaks evolving with the pressure is presented in the background. The Raman scattering spectra of BTFO samples under atmospheric pressure are confirmed to be single phase. The frequencies of most phonon modes increase with the pressure. The applied pressure

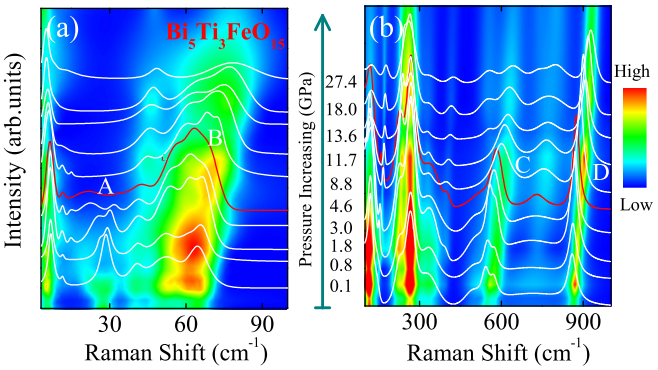

FIG. 1. Raman spectra and intensity mapping of Raman scattering for BTFO from ambient up to 27.4 GPa at different frequencies: (a) 5–100 cm^{-1} and (b) 100–1000 cm^{-1}.

causes the collective movement to slightly distorted octahedral oxygen. However, the frequencies of phonon modes at 265.4 and 146.5 cm^{-1} remain constant. As we know, different phonon modes have different sensitivity to the pressure. All phonon modes can specify the relative origin. The phonon modes with the frequency under 200 cm^{-1} are associated with the Bi atomic vibration. Phonon modes at the frequency of 32.1, 52.5, and 65.6 cm^{-1} are derived from Bi atomic vibration in the Bi_2O_2 layer.[24] The Raman phonon modes at 118.8 and 150.9 cm^{-1} are closely associated with the vibrations of Bi^{3+} at the A-site of the perovskite-like slabs. The modes with the frequency beyond 200 cm^{-1} are all related to the internal vibration of the oxygen octahedron.[25] For example, the phonon mode at 226.0 cm^{-1} is related to the bending and vibration of the O–Ti/Fe–O bond in the oxygen octahedron.[25,26] Phonon modes at 265.4 and 864.0 cm^{-1} with A_{1g} character can distinguish the central atom Ti or Fe in the oxygen octahedron.[27,28] However, the frequency of the mode at 864.0 cm^{-1} shifted significantly under the pressure, suggesting that the $(Ti/Fe)O_6$ octahedron has different effects on the torsional, bending, or stretching behavior of the oxygen octahedron of different central atoms during the structural phase transition.

As can be seen from Fig. 1, the frequency and the intensity of the Raman peak in BTFO ceramics changed with the increasing pressure. In the following discussion, we address the bands by referring to the wavenumber at 0 GPa. The phonon mode at 265.1 cm^{-1} presents the highest intensity in the pressure range of 0–27.4 GPa. First of all, the significant changes in frequency in the peaks (the peaks marked by A, B, C, and D) can be observed between 4.5 and 14.8 GPa. Other obvious aspects can be seen: (A) the mode at 32.1 cm^{-1} splits into two modes with the increasing pressure. With the pressure further increasing, the two modes annihilated around 4.5 GPa; (B) in the pressure range of 0–14.8 GPa, the phonon mode changes from 65.6 cm^{-1} to 72.5 cm^{-1} gradually; (C) when the pressure increases to 4.5 GPa, the modes at 504.1 and 552.7 cm^{-1} are combined into the phonon mode 581.6 cm^{-1}. In the pressure range of 4.5–14.8 GPa, the phonon mode moved from 581.6 to 603.2 cm^{-1}. (D) Under the stress field of 0–14.8 GPa, the phonon mode slowly moves to 892.7 cm^{-1} for a frequency of 870.3 cm^{-1}. To sum up, the lattice symmetry of BTFO changes in the pressure range of 0–14.8 GPa. It is known that any static and/or dynamic changes in the structure should give rise to a

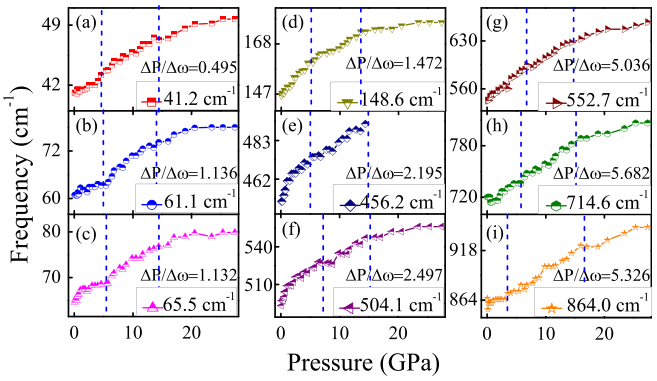

FIG. 2. Pressure dependence of phonon modes: (a) 41.2 cm^{-1}, (b) 61.1 cm^{-1}, (c) 65.6 cm^{-1}, (d), 148.6 cm^{-1}, (e) 456.2 cm^{-1}, (f) 504.1 cm^{-1}, (g) 552.7 cm^{-1}, (h) 714.6 cm^{-1}, and (i) 864.0 cm^{-1} from 0 to 27.4 GPa. The dotted line indicates two different pressure points of 4.5 GPa and 14.8 GPa, respectively.

variation of the phonon behavior.[29,30] Therefore, the analysis of the mode position is expected to give insight into those changes. The frequency changes of the typical phonon modes extracted from Raman scattering spectra are shown in Fig. 2. In general, due to the volume compression of the lattice, the frequency of the phonon mode shifts toward higher frequencies as the pressure increases. In Fig. 2, we observed that all phonon modes move to higher frequencies upon increasing the pressure in the range of 0–27.4 GPa. The phenomenon is caused by the reduction in the distance between atoms. This feature may be related to decreased crystallinity or increased disorder.[31] Figure 2 shows the frequency change with the stress field. Note that the slope of the curve changes around the pressure values of 4.5 GPa and 14.8 GPa. There may be a phase transition in the pressure range of 4.5 GPa–14.8 GPa. It was reported that BTFO ceramics undergo a phase transition when the temperature rises to the Curie temperature: the ferroelectric orthorhombic phase becomes a paraelectric tetragonal phase. We think that BTFO ceramics have such structural phase transition behavior under high pressure. The value of $\Delta P/\Delta\omega$ is the rate of change of frequency between 4.5 and 14.8 GPa. Figures 2(a)–2(d) show that the parameter is related to the bismuth oxide layer and the calculated value of $\Delta P/\Delta\omega$ is less than 2. The vibration of the phonon modes in Figs. 2(e)–2(i) is related to the oxygen octahedron. $\Delta P/\Delta\omega$ is greater than 2. The results indicate that the oxygen octahedron in BTFO is more sensitive to pressure than the bismuth oxide layer. It is worth mentioning that when the stress field is removed, the original Raman spectra can be restored.

In order to verify the phase transition, the intensity and FWHM of the phonon modes are summarized in Fig. 3. The phonon modes at 265.4, 337.5, and 566.6 cm^{-1} are designated as A_{1g} character, and the Raman mode at 870.3 cm^{-1} is designated as B_{1g} character. The intensity of the phonon module slowly decreases with the pressure. When the pressure exceeds 4.5 GPa, the phonon mode at 581.6 cm^{-1} disappears. In Figs. 3(a)–3(g), the phonon modes are related to the oxygen octahedron with the central atom of Ti, where the arrow marked indicates the phonon mode with a sudden increase in intensity at about 15.9 GPa. In Fig. 3(h), the phonon mode is related to the oxygen octahedron with the central atom Fe. When the pressure is about 13.5 GPa, the intensity of the phonon mode is marked as the arrow suddenly increases. With the pressure varying from 0 to 27.4 GPa, the FWHM of the phonon mode at 226.0, 265.4, 337.5, and 504.1 cm^{-1} varies by 5–8 cm^{-1}. The change in the FWHM of the phonon modes at 566.6, 714.6, and 870.3 cm^{-1} is about 25 cm^{-1}. In Figs. 3(a′)–3(h′), the arrow marks the location of the FWHM change. Due to the deformation and volume shrinkage of the BTFO lattice from the stress field, both the phonon mode frequency and the FWHM exhibit changes around the pressure points of 4.5 and 14.8 GPa. The results confirmed the existence of structural transformation under high pressure.

We carried out the *in situ* angle-dispersive XRD experiments under the stress field. Figure 4(a) shows the XRD pattern of BTFO ceramics under different pressures of 0–34.0 GPa. In the stress field, the unit cell is compressed. As the grain size becomes smaller, the x-ray dispersion effect becomes obvious, and the intensity of the diffraction peak decreases. The shift of the phonon mode and the

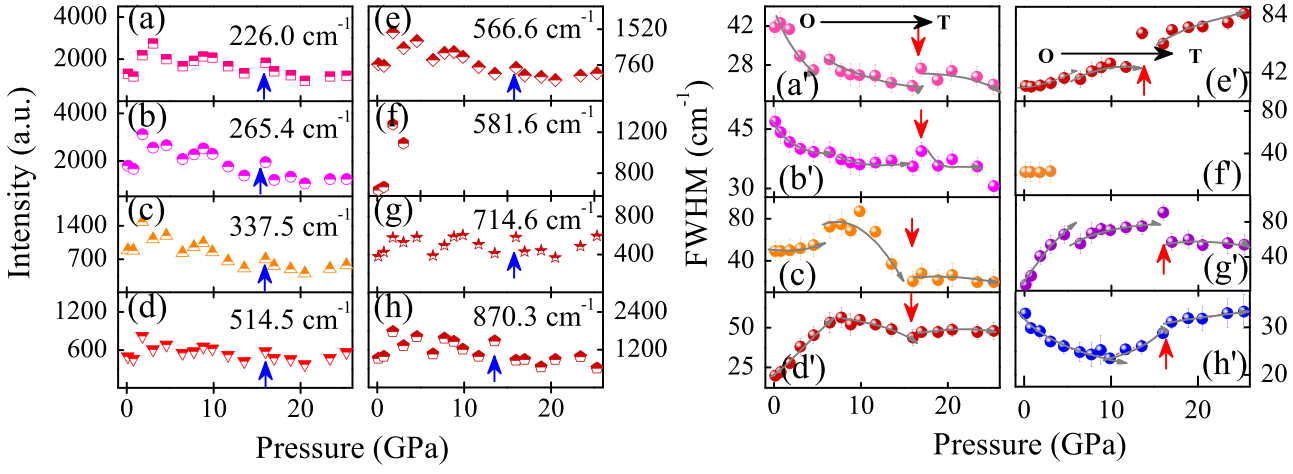

FIG. 3. Intensity and full width at half maximum corresponding to different phonon modes: (a) and (a′) 226.0 cm^{-1}, (b) and (b′) 265.4 cm^{-1}, (c) and (c′) 337.5 cm^{-1}, (d) and (d′) 514.5 cm^{-1}, (e) and (e′) 566.6 cm^{-1}, (f) and (f′) 581.6 cm^{-1}, (g) and (g′) 714.6 cm^{-1}, and (h) and (h′) 870.3 cm^{-1}. Note that the pressure range varies from 0 to 27.4 GPa, and the arrows show the point where the intensity and the FWHM of the phonon mode change.

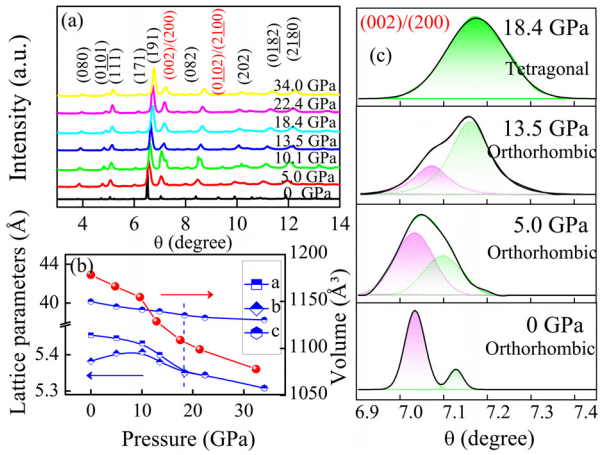

FIG. 4. (a) *In situ* high-pressure angle-dispersive XRD spectrum with the pressure range of 0–34.0 GPa; (b) lattice parameter and volume parameter of the BTFO ceramics at different pressures. (c) The XRD peak angle of the crystal plane index at (002)/(200) evolves with the pressure at 18.4 GPa, 13.5 GPa, 5.0 GPa, and 0 GPa.

diffraction peak indicate the lattice volume compression. In the absence of a stress field, the XRD diffraction peak is consistent with standard card PDF No. 38–1257, proving that the BTFO sample is of single phase. No other diffraction peaks except for that of the BTFO can be detected. The crystal symmetry and unit cell parameters were refined from experimental data Rietveld. The space group belongs to *I*4/*mmm*. The cell parameters (in Å) are $a = 5.4541(1)$, $b = 5.3820(4)$, and $c = 40.1441(1)$. In addition, in order to study the influence of pressure on the microstructure, it can be seen from Fig. 4(b) that the lattice parameters *a*, *b*, and *c* decrease with the increasing pressure. Under the stress field, the crystal cell will be compressed. The distance between the crystal planes will decrease, and the diffraction peak will move to a higher angle.[32–35] When the pressure ranges from 0 to 34.0 GPa, the unit cell volumes of BTFO were calculated to be 1178.4, 1166.1, 1154.6, 1128.8, 1109.0, 1098.9, and 1077.9 $Å^3$. As the grain size decreases under the pressure, the diffusion effect on x-ray becomes obvious, which can result in the fact that the peak widens and the peak strength weakens. As shown in Fig. 4(c), the angles of the XRD diffraction peaks at (200) and (020) become larger as the stress field increases until the diffraction angles are equal. We reprocessed the x-ray experimental data using software Fullprof with the WinPLOTR module. The highly symmetric oxygen site was used as the reference coordinate. The pressure factor of the Ti/Fe cation did not show stability during the increase in the pressure, and its standard deviation was not significantly lower than its value or variation value. Therefore, these parameters are fixed. The pressure is 18.4 GPa, and a satisfactory convergence is achieved. Also, the spatial group *I*4/*mmm* is obtained. Combining the XRD diffraction peaks and Raman spectra, the effects from the pressure appear around 4.5 GPa, indicating that the lattice structure of the BTFO sample was the orthorhombic phase and began to distort. It can be concluded that the phase transition occurs in the pressure range of 14.8–18.4 GPa: orthorhombic phase–tetragonal phase.

In conclusion, we mainly studied the structural phase transition of BTFO ceramics based on pressure-dependent Raman spectroscopy. It was found that the frequencies, intensities, and FWHM of some typical phonon modes changed regularly under the pressure of 4.5–14.8 GPa and the phase transition occurs: orthorhombic phase–tetragonal phase. To further prove the symmetrical change path, a synchrotron XRD experiment was carried out. When the lattice is compressed under applied pressure, the lattice constant and volume fraction decrease. When the pressure reaches 18.4 GPa, the structure of BTFO transforms from orthorhombic $A2_1am$ into tetragonal *I*4/*mmm*, and the cell parameters are equal. Finally, the phase transition path of BTFO ceramics under high pressure can be readily determined.

This work was financially supported by the National Key Research and Development Program of China (Grants Nos. 2018YFB0406500, 2017YFA0303403, and 2019YFB2203400), the National Natural Science Foundation of China (Grants Nos. 91833303, 61974043, 61805081, and 61674057), the Projects of Science and Technology Commission of Shanghai Municipality (Grant Nos. 18JC1412400, 18YF1407200, 18YF1407000, and 19511120100), and the Program for Professor of Special Appointment (Eastern Scholar) at Shanghai Institutions of Higher Learning. The work concerning *in situ* angular dispesion XRD measurements was performed at beamline 15U1, Shanghai Synchrotron Radiation Facility (SSRF).

DATA AVAILABILITY

The data that support the findings of this study are available from the corresponding author upon reasonable request.

REFERENCES

[1]H. Y. Zhao, H. Kimura, Z. X. Cheng, M. Osada, J. L. Wang, X. L. Wang, S. X. Dou, Y. Liu, J. D. Yu, T. Matsumoto, T. Tohei, N. Shibata, and Y. C. Ikuhara, Sci. Rep. **4**, 5255 (2015).
[2]T. T. Jia, H. Kimura, Z. X. Cheng, H. Y. Zhao, Y. Kim, M. Osada, T. Matsumoto, N. Shibata, and Y. Ikuhara, NPG Asia Mater. **9**, e349 (2017).
[3]A. Y. Birenbaum and C. Ederer, Phys. Rev. B **90**, 214109 (2014).
[4]R. E. Newnham, R. W. Wolfe, and J. F. Dorrian, Mater. Res. Bull. **6**, 1029–1039 (1971).
[5]E. K. H. Salje, E. Dul'Kin, and M. Roth, Appl. Phys. Lett. **106**, 152903 (2015).
[6]S. Nakashima, T. Uchida, D. Nakayama, H. Fujisawa, M. Kobune, and M. Shimizu, Jpn. J. Appl. Phys., Part 1 **53**, 09PA16 (2014).
[7]C. H. Hervoches, J. T. S. Irvine, and P. Lightfoot, Phys. Rev. B **64**, 100102 (2001).
[8]P. F. Zhang, N. Deepak, L. Keeney, M. E. Pemble, and R. W. Whatmore, Appl. Phys. Lett. **101**, 112903 (2012).
[9]S. X. Yan, Z. W. Feng, Z. M. Ma, Y. C. Zhang, and W. N. Ye, Mater. Lett. **227**, 247–249 (2018).
[10]K. Tang, W. Bai, J. Liu, J. Yang, Y. Y. Zhang, C. G. Duan, X. D. Tang, and J. H. Chu, Ceram. Int. **41**, S185–S190 (2015).
[11]P. Durân, F. Capel, C. Moure, M. Villegas, J. F. Fernândez, J. S. Tartaj, and A. C. Caballero, Ceram. Int. **21**, 1–8 (2001).
[12]F. Kubel, H. Schmid, M. X. Yu, and C. X. Bing, J. Ferroelectr. **129**, 101–112 (1992).
[13]G. A. Samara, T. Sakudo, and K. Yoshimitsu, Phys. Rev. Lett. **35**, 1767–1769 (1975).
[14]A. Snedden, C. H. Hervoches, and P. Lightfoot, Phys. Rev. B **67**, 092102 (2003).
[15]W. Cochran, Phys. Rev. Lett. **3**, 412 (1959).
[16]W. Cochran, Adv. Phys. **9**, 387 (1960).
[17]J. B. Li, Y. P. Huang, G. H. Rao, G. Y. Liu, J. Luo, J. R. Chen, and J. K. Liang, Appl. Phys. Lett. **96**, 222903 (2010).
[18]K. Lynette, G. Claudia, K. Santosh, R. Saibal, M. E. Pemble, and R. W. Whatmore, J. Appl. Phys. **112**, 024101 (2012).

[19]D. A. Mota, A. Almeida, V. H. Rodrigues, M. M. R. Costa, P. Tavares, P. Bouvier, M. Guennou, J. Kreisel, and J. A. Moreira, Phys. Rev. B **90**, 054104 (2014).
[20]G. Chen, W. Bai, L. Sun, J. Wu, Q. Ren, W. Xu, J. Yang, X. J. Meng, X. D. Tang, C. G. Duan, and J. H. Chu, J. Appl. Phys. **113**, 034901 (2013).
[21]R. Ti, X. Lu, J. He, F. Huang, H. Wu, F. Mei, M. Zhou, Y. Li, T. Xu, and J. Zhu, J. Mater. Chem. C **3**, 11868–11873 (2015).
[22]H. Idink, V. Srikanth, W. B. White, and E. C. Subbarao, J. Appl. Phys. **76**, 1819 (1994).
[23]J. Kreisel, A. M. Glazer, P. Bouvier, and G. Lucazeau, Phys. Rev. B **63**, 174106 (2001).
[24]S. Kojima, R. Imaizumi, S. Hamazaki, and M. Takashige, Jpn. J. Appl. Phys., Part 1 **33**, 5559–5564 (1994).
[25]B. Jiang, M. H. Tang, J. C. Li, Y. G. Xiao, H. Z. Tao, Y. C. Zhou, and J. He, J. Electron. Mater. **41**, 651–655 (2012).
[26]V. Koval, I. Skorvanek, J. Durisin, G. Viola, A. Kovalcikova, P. Svec, Jr., K. Saksl, and H. X. Yan, J. Mater. Chem. C **5**, 2669–2685 (2017).
[27]K. Liang, Y. Qi, and C. Lu, J. Raman Spectrosc. **40**, 2088–2091 (2009).
[28]F. Z. Huang, X. M. Lu, T. T. Xu, Y. Y. Liu, W. N. Su, Y. M. Jin, Y. Kan, and J. S. Zhu, Thin Solid Films **520**, 6489–6492 (2012).
[29]C. B. Long, H. Q. Fan, and P. R. Ren, Inorg. Chem. **52**, 5045–5054 (2013).
[30]R. J. Angel, J. Zhao, and N. L. Ross, Phys. Rev. Lett. **95**, 025503 (2005).
[31]T. D. Kang, E. C. Standard, P. D. Rogers, K. H. Ahn, A. A. Sirenko, A. Dubroka, C. Bernhard, S. Park, Y. J. Choi, and S. W. Cheong, Phys. Rev. B **86**, 144112 (2012).
[32]S. Tongsang, J. Padchasri, J. Jutimoosik, A. Bootchanont, S. Rujirawat, and R. Yimnirun, Ferroelectrics **552**, 172–176 (2019).
[33]R. Vilarinho, P. Bouvier, M. Guennou, I. Peral, M. C. Weber, P. Tavares, M. Mihalik, Jr., M. Mihalik, G. Garbarino, M. Mezouar, J. Kreisel, A. Almeida, and J. A. Moreira, Phys. Rev. B **99**, 604109 (2019).
[34]V. Panchal, N. Garg, H. K. Poswal, D. Errandonea, P. Rodríguez-Hernández, À. Muoz, and E. Cavalli, Phys. Rev. Mater. **1**, 043605 (2017).
[35]P. P. Jiang, X. L. Zhang, P. Chang, Z. G. Hu, W. Bai, Y. W. Li, and J. H. Chu, J. Appl. Phys. **115**, 144101 (2014).